Physica Scripta. Vol. 37, 645–650, 1988.

# Interpretation of the Structure of Mesospheric Turbulence Layers in Terms of Inertia Gravity Waves

Mamoru Yamamoto, Toshitaka Tsuda, Susumu Kato, Toru Sato and Shoichiro Fukao

Radio Atmospheric Science Center, Kyoto University, Uji, Kyoto 611 Japan

*Received September 15, 1986; accepted April 6, 1987*

**Abstract**

MU radar observations with good time-height resolution have found that inertia gravity waves play an important role in producing turbulence layers in the mesosphere. When the Richardson number modified by the inertia gravity wave was larger than 1, the inertia gravity wave confined the altitude region with relatively small Richardson number, where smaller scale perturbations superposed on the wave seemed to make the Richardson number smaller than the critical values for instabilities, and produce turbulence. Scattering layers showed a descending motion at a vertical phase velocity of a monochromatic inertia gravity wave, and appeared at the altitude of the minimum Richardson number modified by the wave. A mixture of several layers with different descending motions was observed when wind fields consist of several gravity waves with different vertical wavelengths and phase velocities. On the other hand, when the Richardson number modified by the inertia gravity wave became as small as 0, the wave itself seemed to be dissipated through instabilities, and produce thicker turbulence layer than that in other cases. The radial wind velocities showed large fluctuations with a period of 9 min, which showed a phase reversal near the altitude of minimum Richardson number. The fluctuation seemed to be attributed to the shear instability induced by the saturated inertia gravity wave.

## 1. Introduction

MST radar observations performed at VHF have revealed that mesospheric turbulence regions are distributed discontinuously in time and space [1, 2]. By the SOUSY radar observations with height resolution of 150 m, various structures of turbulence regions have been classified into blobs, sheets and layers [3] although the mechanism to produce the different structures is not explained. Also, it is observed that the height intervals of the scattering layers are associated with the half of the vertical wavelength of the wave-like structure in the wind field, and the maximum echo power appears around the altitude of the maximum vertical wind shear [4, 5]. Observations in the mesosphere [6–8] have shown that gravity waves are dissipated through dynamical or convective instabilities [9, 10]. It is theoretically expected that gravity waves in the upper mesosphere are saturated, and produce turbulence. In this paper, we have investigated a relation between gravity waves and scattering layers by using MU radar observations.

## 2. MU radar observations

The MU radar (35°N, 136°E) completed in 1984 is described in detail by Kato *et al.* [11] and Fukao *et al.* [12, 13]. We have observed the mesosphere in two observational periods on the 8 February 1985 and on the 13 and 14 February 1986. Fundamental observation parameters are listed in Table I. The major differences between the two observations are range resolution and number of beam directions. The range resolution was 300 m in the first observation, while it was 600 m with 300 m oversampling in the second observation. We have observed only four oblique directions at a zenith angle of 10° in the first observation, and vertical and four oblique directions in the second observation. Echo power, radial wind velocity and spectral width are determined by a least square fitting of Doppler spectra. Horizontal wind velocities are calculated from a pair of radial wind velocity measurements in the opposite beam directions.

Table I. *Observation parameters*

| Observation period | 13, 14 February 1986 | 8 February 1985 |
|---|---|---|
| Observation range | 60–98.1 km | 60–98.1 km |
| Beam directions | Vertical | Northward ($\theta$ = 10°) |
| ($\theta$: Zenith angle) | Northward ($\theta$ = 10°) | Eastward ($\theta$ = 10°) |
| | Eastward ($\theta$ = 10°) | Southward ($\theta$ = 10°) |
| | Southward ($\theta$ = 10°) | Westward ($\theta$ = 10°) |
| | Westward ($\theta$ = 10°) | |
| Range resolution | 600 m | 300 m |
| | (sampled every 300 m) | |
| Time resolution | 150 s | 120 s |
| Inter pulse period | 730 $\mu$s | 730 $\mu$s |
| Pulse compression | 8 bit complementary | 16 bit complementary |
| Coherent integration | 20 times | 30 times |
| Incoherent integration | 6 times | 10 times |

## 3. Results

From MU radar observations of the mesosphere, we have frequently found evidence of inertia gravity waves with periods around 10 h and vertical wavelengths ranging from 4 to 20 km. Inertia gravity waves significantly modify the Richardson number profile through modifications of both wind shear and temperature profiles [10, 14]. We have studied relations between structure of scattering layers and Richardson number profiles modified by inertia gravity waves. In the calculation of the Richarson number profile, we have assumed the wind fields as a superposition of inertia gravity waves on a linear background shear. Perturbation of potential temperature due to gravity waves is estimated by using the linear polarization equation of gravity waves between wind velocity and temperature variation [10]. We have adopted the CIRA 1972 [15] model as a background potential temperature profile.

### 3.1. *A monochromatic inertia gravity wave with minimum Richardson number > 1*

Figure 1 shows eastward wind profiles determined in every 2 h at each altitude accompanied with a background linear trend averaged over 8–16 LT and smoothed wind profiles

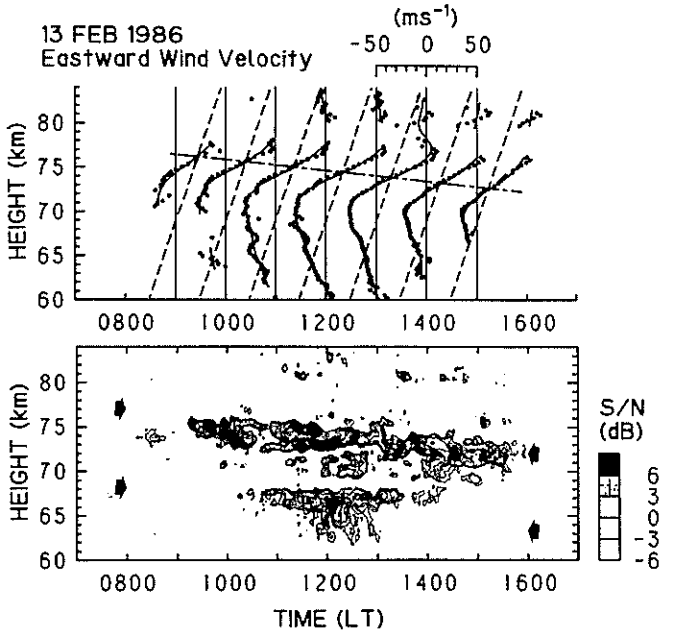


*Fig. 1.* Wind profiles (top) and echo power contour (bottom) observed on 13 February 1986. Dots in the top panel show eastward wind profiles each of which is a 2 h average determined every 1 h. Dashed lines show a vertical linear trend of the wind profile averaged over the whole observation period. Thick curves denote wind profiles after low-pass filtering with a cutoff wavelength of 6 km. A chained line indicates a phase line connecting points where filtered wind profile go across the linear trend. Two pairs of arrows in the bottom panel correspond to the phase lines with vertical spacing of half of the wavelength of the inertia gravity wave.

obtained by removing fluctuations with wavelengths smaller than 6 km by a low-pass filter. A wave-like structure with a vertical wavelength of approximately 18 km is recognized in the filtered wind profile, which suggests a manifestation of an inertia gravity wave. A phase line, which is determined by connecting points where the profiles go across the linear trend wind, clearly shows a downward progression of phase. The vertical phase velocity is estimated as 0.6 km/h. Fig. 1 also shows that intense scattering layers at the 70–75 km altitudes distribute discretely in height with thickness of a few kilometers, and propagate downward. The upper pair of arrows in the echo power contour at 72–77 km altitudes indicates locations of the phase line drawn in the wind profiles. The lower pair of arrows are shifted downward by half of the vertical wavelength of the gravity wave. The progression of the structure of the scattering layers at 70–75 km is almost parallel to the downward propagation of the wind fields. The other intense scattering layer at 63–68 km centered at noon appears around the phase line indicated by the lower pair of the arrows, but does not show clear downward motion.

In order to investigate the polarization of the wave, a wind velocity vector is calculated by averaging the eastward and northward components during 12–14 LT. Figure 2 shows a hodograph of the wind vector after subtracting the vertical linear trend of the wind. The tip of the wind vector moves clockwise with increasing height. By removing components with vertical wavelength smaller than 6 km, the wind vector shows an elliptical rotation, although contaminations by smaller scale fluctuations are still recognized. This shows that the wave is an inertia gravity wave propagating upward [16]. From the ratio between the long and short axes of the ellipse, the intrinsic period of the wave is estimated to be approximately 9.7 h. The direction of the long axis shows that the

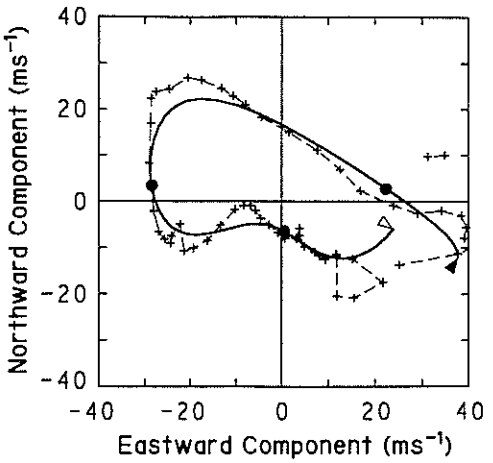


*Fig. 2.* A polar plot of the wind fields observed in 12–14 LT on 13 February 1986. Cross symbols show determinations of wind vectors at each altitude. Vertical linear trend of the wind profile is extracted. The smoothed curve is obtained by using the low-pass filter with a cutoff wavelength of 6 km. The open and solid triangles on the solid line indicate the lowest (60.2 km) and highest altitudes (77.5 km). Circular symbols are plotted at 65, 70 and 75 km.

wave seems to propagate horizontally either to the north-west or the south-east. In order to calculate a Richardson number profile modified by the inertia gravity wave, we must determine the propagation direction. According to the polarization equation of gravity waves, the vertical wind component is almost in-phase with the horizontal component along the propagating direction [16]. Unfortunately, the vertical wind velocity in 12–14 LT was not systematic enough to determine the profile. However, the sign of the vertical wind velocities obtained before and after the wind vector determination have suggested that the inertia gravity wave may have propagated to the north-west.

By using the characteristics of the inertia gravity wave in 12–14 LT listed in Table II, a corresponding Richardson number profile is calculated as shown in Fig. 3. It has minimum values of 3.2 and 1.8 at 67 and 73 km altitudes, respectively. Note that the altitudes of the minimum Richardson number do not necessarily agree with those of the maximum wind shear, because the Richardson number profile is also affected by the temperature gradient which has a phase shift to the wind shear profile [10, 14]. Enhancements in the echo

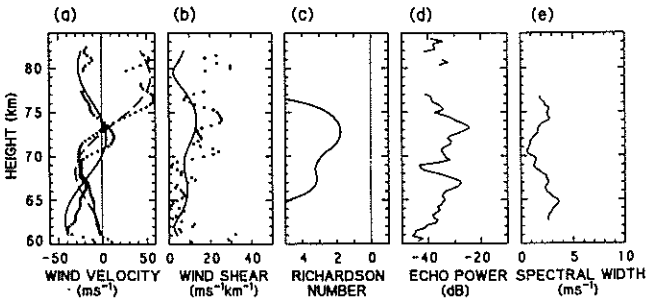


*Fig. 3.* Vertical profiles of (a) wind fields, (b) wind shear, (c) Richardson number, (d) echo power and (e) spectral width observed in 12–14 LT on 13 February 1986. Dots and cross symbols in (a) correspond to northward and eastward wind components averaged over 2 h, respectively. Solid and dashed lines in (a) shows northward and eastward components of the model wind which is obtained by assuming the linear trend and the inertia gravity wave listed in Table II, respectively. Dots in (b) correspond to intensity of vector shear of the observed wind velocities shown in (a), and a solid line to that of the model wind. The Richardson number profile is obtained by using the model wind.

Table II. *Parameters for the Richardson number calculations*

| Observation period | 13 February 1986 | 14 February 1986 | | 8 February 1985 |
|---|---|---|---|---|
| Inertia gravity waves | | (I) | (II) | |
| Intrinsic period (hr) | 9.7 | 8.9 | 9.0 | 8.0 |
| Vertical wavelength (km) | 17.6 | 12.5 | 3.0 | 5.6 |
| Propagating direction | 58° west from the north | 53° west from the north | Westward | 7° east from the north |
| Amplitude* ($m s^{-1}$) | 30.0 | 29.4 | 6.0 | 19.0 |
| Mean background wind | | | | |
| Eastward wind | | | | |
| shear ($m s^{-1} km^{-1}$) | 3.3 | 0.4 | | 4.4 |
| velocity ($m s^{-1}$) at 70 km | 1 | 25 | | 13 |
| Northward wind | | | | |
| shear ($m s^{-1} km^{-1}$) | 0.9 | 2.2 | | 3.7 |
| velocity ($m s^{-1}$) at 70 km | −16 | −8 | | −14 |

* Maximum wind velocity along the long-axis of the ellipse.

power profile detected at 67 and 73 km altitudes coincide with the minima of the Richardson number profile. Also, the minimum of the echo power profile at 69 km corresponds to the altitude of the local maximum of the Richardson number. A vertical profile of spectral width has peaks at around 65 and 75 km, and a broad minimum of about 0.5 $m s^{-1}$ at around 70 km.

As shown in Fig. 3(a), the wind profile averaged over 2 h is well described by the model wind field which is a superposition of the monochromatic inertia gravity wave on the vertical linear trend. The amplitude of the wave does not seem to increase with altitude. This implies that the wave is saturated. However, the minimum value of the Richardson number associated with the wave and mean flow is not small enough to excite either convective or shear instabilities [10]. It is likely that the inertia gravity wave produces regions with relatively small Richardson number, where it may become smaller than the critical values due to the possible superposition of smaller scale fluctuations, and thus turbulence layers are easily produced.

### 3.2. *Superposition of gravity waves with Richardson number > 1*

A similar observation to case 3.1 has been made on 14 February 1986. Wind fields shown in Fig. 4 indicate an inertia gravity wave with a vertical wavelength and downward phase velocity of 12.5 km and 0.8 km/h, respectively. A polar plot of the filtered wind fields is shown in Fig. 5. The elliptical motion of the wind vector indicates that the inertia gravity wave has an intrinsic period of 8.9 h, which is slightly shorter than the inertia gravity wave detected on the previous day. The propagation direction of the wave was determined as in the case 3.1 and was in the north-west direction. This suggests that we have observed the same inertia gravity wave on two consecutive days. However, echo power profiles, also plotted in Fig. 4, show a much more complicated structure than in Fig. 1. Although the over-all structure of intense scattering regions shows downward progression, which seems to agree with the phase line of the inertia gravity wave as indicated by the pair of thick arrows in Fig. 4, the scattering region has fine structures with various time-height scales.

In the 70–76 km region of the wind profile without filtering, another wave-like variation is recognized. The vertical wavelength and downward phase velocity of the wave is approximately 3.0 km and 0.4 km/h respectively. The phase line of this wave is also indicated by the thin arrows in the echo power contour in Fig. 4. Thin turbulence layers at 74 km around 10 LT and at 70–72 km in 13–14 LT seem to show a similar descending motion to the phase line indicated by the thin arrows. In Fig. 5, the wind vector without filtering shows a corresponding elliptical motion superposed on the rotation due to the wave with larger wavelength. The intrinsic period of the wave seems to be approximately 9 h. Considering the vertical component of the wind, this wave seems to propagate westward.

Figure 6 shows the filtered wind profile determined during 10–11 LT and a Richardson number profile calculated by assuming wind fields as a superposition of a linear trend and two gravity waves (I) and (II). As summarized in Table II, we have assumed an inertia gravity wave (I) with wavelength of 12.5 km in the whole altitude range. Another gravity wave (II) with wavelength of 3.0 km is superposed within 69–77 km altitudes in order to approximate fine structure of the wind

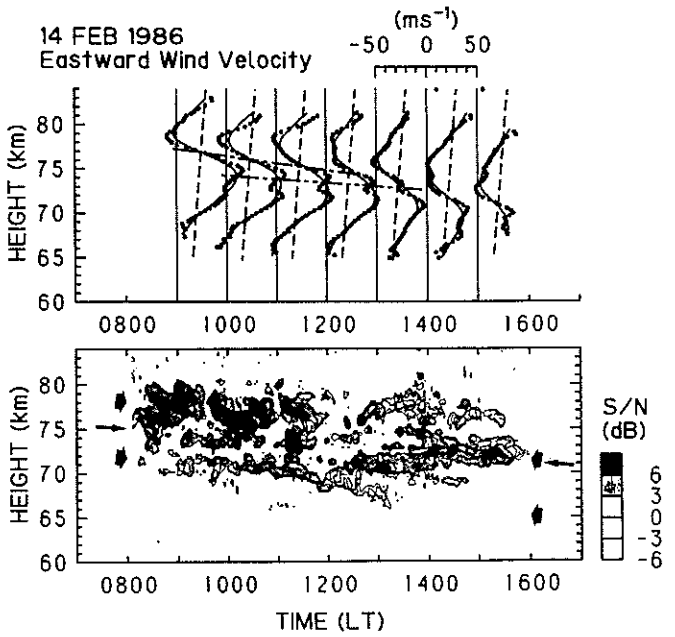


*Fig. 4.* The same as Fig. 1. except for the observations on 14 February 1986. Two kinds of phase lines with downward phase velocities of 0.8 and 0.4 km/h are indicated as chained and double-chained lines(top), and thick and thin arrows (bottom), respectively.

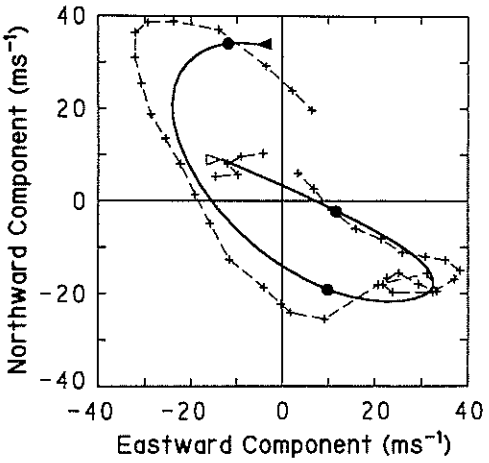


*Fig. 5.* The same as Fig. 2. except for the observations in 10–11 LT on 14 February 1986. The open and solid triangles on the solid line indicates the lowest (67.6 km) and highest altitudes (80.6 km). Circular symbols are plotted at 70, 75 and 80 km.

fields: the amplitude is set to 6 m s$^{-1}$ between 72 and 74 km, and linearly tapered off to 0 m s$^{-1}$ at the 77 and 69 km altitudes. The Richardson number profile has two broad minima of approximately 1.0 in the altitude regions above 75 km and below 71 km, which generally agree with intense peaks of the echo power profile and spectral width. These minima of Richardson number at around 71 and 75 km are attributed to the superposition of the two gravity wave with different wavelengths, and can not be explained by assuming only the larger scale inertia gravity wave. The Richardson number became large at the 73–74 km altitudes where the echo power becomes weak as can be recognized from Fig. 6.

Although the echo power profile shown in Fig. 4 is complicated, its structure seems to be correlated with the behavior of the gravity waves. It might be appropriate to interpret the structures of the scattering regions observed on 14 February 1986 as a superposition of many layers each of which progressed downward following various motions of gravity waves. That is, a mechanism to generate the scattering layer would be the same as that in case 3.1, but superposition of various gravity waves made the structure of scattering layers complicated.

### 3.3. *A monochromatic inertia gravity wave with Richardson number < 1/4*

Figure 7 shows the northward wind profiles and echo power observed on 8 February 1985. Since the averaged northward wind velocities determined every 1 h increase with time, a linear trend of the height profile of the wind field averaged

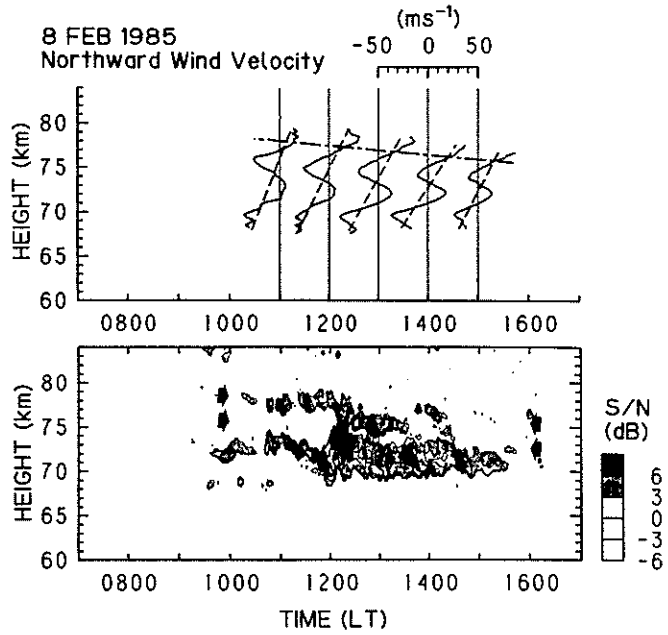


*Fig. 7.* The same as Fig. 1 except for the observations on 8 February 1985. Linear trends are determined using 2 h of observations. Solid lines in the top panel correspond to northward wind velocities without filtering. Smoothed wind profies are not shown.

over the whole observation period, as was used in cases 3.1 and 3.2, is not appropriate to represent the background trend of the wind fields. Therefore, vertical linear trends in Fig. 7 are calculated every wind profile. The wind fields contain a monochromatic inertia gravity wave with a vertical wavelength and downward phase velocity of 5.6 km and approximately 0.5 km/h, respectively. Note that no filtering was applied to the wind profiles. An intrinsic period determined by the actual ratio of short and long axes of the elliptical rotation of the inertia gravity wave is 8 h.

Figure 7 also shows a thick scattering layer at the 69–74 km altitudes, and another layer overlying the thick layer. Although the inertia gravity wave shows clear downward phase progression, the scattering layers do not have a clear corresponding motion, which is not in agreement with the behavior of the scattering layers in cases 3.1 and 3.2. Moreover, the thickness of the layers is much larger than half of the wavelength of the inertia gravity wave. Fine structures of the intense turbulence regions centered at 72 km at 12 LT show rapid time-height variations.

The Richardson number profile is shown in Fig. 8, where the wind velocities were well approximated by a single inertia gravity wave. It is interesting that the Richardson number due to the inertia gravity wave becomes smaller than 0 at 72 and 77.5 km altitudes where the horizontal wind vector of the

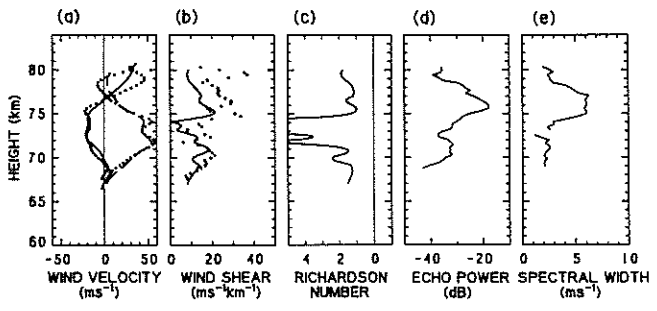


*Fig. 6.* The same as Fig. 3 except for the observations in 10–11 LT on 14 February 1986.

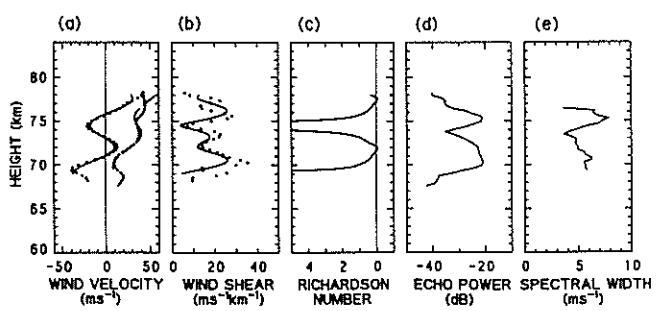


*Fig. 8.* The same as Fig. 3 except for the observations in 12:30–13:30 LT on 8 February 1985.

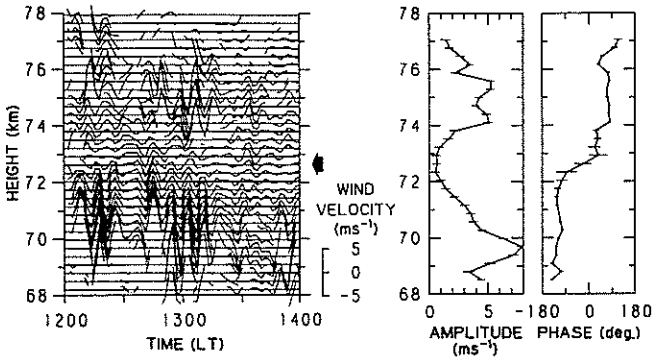


*Fig. 9.* Fluctuations of radial wind velocities with periods ranging from 6 to 16 min in the southward direction at zenith angle of 10° (left panel), and vertical profiles of amplitude (center panel) and phase (right panel) of the fluctuation with a period of 9 min detected in 12:58–13:21 LT. The bars on the amplitude and phase profiles show estimation errors. An arrow indicates the altitude of the phase reversal determined from the phase profile.

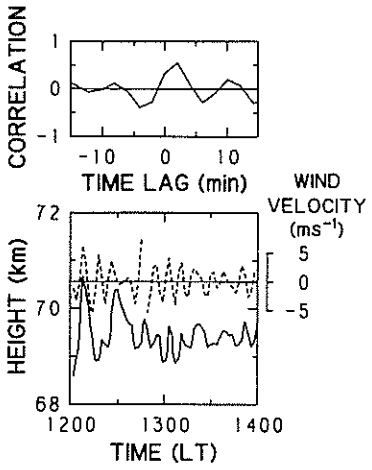


*Fig. 10.* Altitude variation of scattering layer and radial wind velocities in the southward bean (bottom). A solid line shows the altitude variation of the constant signal to noise ratio (−3 dB) around 69.5 km shown in Fig. 7. A dashed line corresponds to the variation of the radial wind velocities at 70.6 km. Top panel shows cross-correlation coefficient between altitude variation and the radial velocities shown in the bottom panel. Positive lag shows that the altitude variation of the scattering layer lags relative to the radial velocities.

inertia gravity wave becomes parallel to the horizontal propagation direction, and has a maximum speed with minimum wind shear. The inertia gravity wave itself seems to be dissipated, because the Richardson number due to the inertia gravity wave is smaller than the critical values for onsets of shear and convective instabilities. The minimum of the Richardson number at around 72 km coincides with an enhancement of the echo power, while there is a difference in altitude by a few kilometers between the minimum of Richardson number and the peak of the echo power in the upper altitude region.

Figure 9 shows radial wind velocities observed in the southward direction at a zenith angle of 10°, where fluctuations with periods ranging from 6 to 16 min are selected by a band pass filter. It is clear that an intense intermittent oscillation with a period of approximately 9 min was observed in the altitude regions lower than 72 km and higher than 74 km. The phase profile which is determined in 12:58–13:21 LT by assuming a sinusoidal oscillation with a period of 9 min indicates that the phases are reversed at 72.7 km where the Richardson number was almost at a minimum. Estimation errors of both amplitude and phase are indicated by the bars on the profiles, and relatively small. Phase values are nearly constant in both regions upper and lower of the altitude of the phase reversal. The amplitude profile shows a minimum at around 73 km, and maxima at altitudes of 75 and 69 km. This behavior of the wind fluctuations agree well with the characteristics of the Kelvin–Helmholtz instability observed in the troposphere [17, 18]. It is likely that the dissipated inertia gravity wave excites the shear instability, and eventually produces turbulence regions. Intense peaks of the echo power and spectral width at around 75 km shown in Fig. 8 seem to agree with those recognized in the amplitude profile in Fig. 9.

From the echo power contour in Fig. 7, it can be recognized that the lower edge of the turbulence layer at around 70 km in 12–14 LT showed an oscillation with a period similar to the wind fluctuation in Fig. 9. Figure 10 shows the variation of altitudes with a constant signal to noise ratio of −3 dB, and radial wind velocity due to small scale fluctuations at 70.6 km altitude. A cross-correlation between these fluctuations shows that the altitude fluctuation of the turbulence layer lags the radial wind fluctuation by approximately 2 min. Because the period of the fluctuation is 9 min, the altitude of the lower edge seems to lag approximately 90° relative to the radial velocity. This seems to be a modulation of the turbulence layer due to the instabilities observed in the radial wind field. Mesospheric observations of the SOUSY radar have shown echo power bursts associated with the vertical wind fluctuations [4, 5, 19]. However, we can not find clear evidence for turbulence generated by these wind fluctuations.

## 4. Concluding remarks

We have studied behavior of inertia gravity waves in the upper mesosphere by the MU radar observations with a height resolution of 300–600 m. Time-height variation of the scattering layers are also monitored with a time resolution of 2–2.5 min. The amplitudes of the inertia gravity waves did not seem to increase with height, which implies that the waves are saturated and lose their energy. It is found that the scattering layers are detected at the altitudes of small Richardson number modified by the inertia gravity waves. When the amplitude of the inertia gravity wave is relatively small, that is the minimum Richardson number associated with the wave is larger than 1, the wave generates a narrow altitude region with smaller Richardson number relative to those in the surrounding altitudes. Smaller scale gravity waves superposed on the inertia gravity wave give further modifications of the Richardson number, and generate turbulence regions by dissipating themselves through shear or convective instabilities. Cases 3.1 and 3.2 correspond to the condition described above. When a monochromatic inertia gravity wave is dominant in the wind fields, scattering regions in case 3.1 look like layers in the classification of turbulence structures by Röttger [3]. In case 3.2, we have shown a superposition of scattering layers attributed to various gravity waves, which would be observed as a single thick region if they were observed by an MST radar with height resolution poorer than that used in this study. Differences in structures of the scattering layers in cases 3.1 and 3.2 seem to be attributed to characteristics of the wind fields determined by the gravity waves.

On the other hand, the Richardson number induced by the inertia gravity waves sometimes becomes smaller than the critical values for instabilities. In case 3.3, which corresponded to this condition, we have observed systematic wind fluctuations due to shear instability as shown in Fig. 9 at the altitudes near minimum of the Richardson number. The inertia gravity wave itself seems to be saturated and is dissipated through instabilities, thus producing turbulence. It should be noted that we have not observed the phase reversal in the radial wind fluctuations in cases 3.1 and 3.2, and the amplitudes of the fluctuations are less than that in this case. Considering the vertical wavelength of the wave, the scattering region of this case is much thicker than those which are confined in the altitudes with the relatively small Richardson number as shown in other cases. Also, we have recognized fine structures in the scattering region in Fig. 7. The intense patchy structures could be interpreted as blobs in Röttger's classification [3].

From these observations, we have found clear evidence that the structures of the mesospheric scattering layers are related to the activity of the inertia gravity waves. Especially, the vertical thickness of the scattering region seems to be associated with the spatial or time scale of the wave which is actually dissipated into turbulence. This study have shown that inertia gravity waves propagating upward from lower atmosphere saturate in the upper mesosphere, and play important role in depositing their energy into turbulence by shear or convective instabilities.

## Acknowledgement

The authors wish to thank Dr. P. T. May for helpful suggestions. The MU radar belongs to and is operated by Radio Atmospheric Science Center, Kyoto University.

## References

1. Harper, R. M. and Woodman, R. F., J. Atmos. Terr. Phys. **39**, 959 (1977).
2. Czechowsky, P., Rüster, R. and Schmidt, G., Geophys. Res. Lett. **6**, 459 (1979).
3. Röttger, J., Rastogi, P. K. and Woodman, R. F., Geophys. Res. Lett. **6**, 617 (1979).
4. Rüster, R., Adv. Space Res. **4**, 3 (1984).
5. Rüster, R. and Klostermeyer, J., Handbook for MAP **18**, 216 (1985).
6. Manson, A. H., Meek, C. E. and Stening, R. J., J. Atmos. Terr. Phys. **41**, 325 (1979).
7. Vincent, R. A. and Stubbs, T. J., Planet. Space Sci. **25**, 441 (1977).
8. Vincent, R. A., J. Atmos. Terr. Phys. **46**, 119 (1984).
9. Fritts, D. C., Rev. Geophys. **22**, 275 (1984).
10. Fritts, D. C. and Rastogi, P. K., Radio Sci. **20**, 1247 (1985).
11. Kato, S., Ogawa, T., Tsuda, T., Sato, T., Kimura, I. and Fukao, S., Radio Sci. **19**, 1475 (1984).
12. Fukao, S., Sato, T., Tsuda, T., Kato, S., Wakasugi, K. and Makihira, T., Radio Sci. **20**, 1155 (1985).
13. Fukao, S., Tsuda, T., Sato, T., Kato, S., Wakasugi, K. and Makihira, T., Radio Sci. **20**, 1169 (1985).
14. Tsuda, T., Hirose, K., Kato, S. and Sulzer, M. P., Radio Sci. **20**, 1503 (1985).
15. CIRA, COSPAR International Reference Atmosphere, Akademie-Verlag, Berlin (1972).
16. Gossard, E. E. and Hooke, W. H., Waves in the Atmosphere, p. 111, Elsevier, New York (1975).
17. Klostermeyer, J. and Rüster, R., J. Geophys. Res. **85**, 2841 (1980).
18. VanZandt, T. E., Green, J. L., Clark, W. L. and Grant, J. R., Geophys. Res. Lett. **6**, 429 (1979).
19. Klostermeyer, J. and Rüster, R., Adv. Space Res. **4**, 79 (1984).